



**HAL**  
open science

## Structural properties and polarization switching of epitaxial $\text{Bi}_2\text{FeCrO}_6$ thin films grown on $\text{La}_{2/3}\text{Sr}_{1/3}\text{MnO}_3/\text{SrTiO}_3$ (111) substrates

Laurianne Wendling, Xavier Henning, François Roulland, Marc Lenertz, Giles Versini, Laurent Schlur, U-Chan Chung, Aziz Dinia, Silviu Colis, Mircea Rastei

### ► To cite this version:

Laurianne Wendling, Xavier Henning, François Roulland, Marc Lenertz, Giles Versini, et al.. Structural properties and polarization switching of epitaxial  $\text{Bi}_2\text{FeCrO}_6$  thin films grown on  $\text{La}_{2/3}\text{Sr}_{1/3}\text{MnO}_3/\text{SrTiO}_3$  (111) substrates. *Thin Solid Films*, 2022, 757, 139384 (6 p.). 10.1016/j.tsf.2022.139384 . hal-03729520

**HAL Id: hal-03729520**

**<https://hal.science/hal-03729520>**

Submitted on 20 Jul 2022

**HAL** is a multi-disciplinary open access archive for the deposit and dissemination of scientific research documents, whether they are published or not. The documents may come from teaching and research institutions in France or abroad, or from public or private research centers.

L'archive ouverte pluridisciplinaire **HAL**, est destinée au dépôt et à la diffusion de documents scientifiques de niveau recherche, publiés ou non, émanant des établissements d'enseignement et de recherche français ou étrangers, des laboratoires publics ou privés.

# Structural properties and polarization switching of epitaxial $\text{Bi}_2\text{FeCrO}_6$ thin films grown on $\text{La}_{2/3}\text{Sr}_{1/3}\text{MnO}_3$ / $\text{SrTiO}_3$ (111) substrates

L. Wendling<sup>1</sup>, X. Henning<sup>1</sup>, F. Roulland<sup>1</sup>, M. Lenertz<sup>1</sup>, G. Versini<sup>1</sup>, L. Schlur<sup>1</sup>, U. Chung<sup>2</sup>, A. Dinia<sup>1</sup>, S. Colis<sup>1</sup>, M.V. Rastei<sup>1</sup>

<sup>1</sup>*Institut de Physique et Chimie des Matériaux de Strasbourg, CNRS, Université de Strasbourg, 23 rue du Loess, F-67034 Strasbourg France*

<sup>2</sup>*Univ. Bordeaux, CNRS, Bordeaux INP, ICMCB, UMR 5026, F-33600 Pessac, France*

## Abstract

*Ferroelectric  $\text{Bi}_2\text{FeCrO}_6$  (BFCO) double perovskite thin films were grown by pulsed laser deposition on  $\text{SrTiO}_3$  (111) covered with a 20 nm thick  $\text{La}_{2/3}\text{Sr}_{1/3}\text{MnO}_3$  buffer layer. X-ray diffraction measurements performed in  $\theta$ - $2\theta$  and  $\varphi$  scans modes reveal an epitaxial growth of the BFCO with a compressive in-plane strained structure and no spurious phases. The presence of superstructure diffraction peaks indicates an Fe-Cr cationic ordering along the growth axis. Local measurements realized by piezo-response force microscopy show an asymmetric polarization switching with respect to the external bias voltage suggesting the presence of a bias field. This agrees with a preferential ferroelectric polarization observed upon local poling of the BFCO film in opposite directions. The findings can be of importance for understanding the relationship between the atomic structure and polarization dynamics in ferroelectric thin-films.*

## Keywords

*Ferroelectricity, Bias Field, Strain, Switching Field, Polarization, Bismuth iron chromium oxide.*

## Introduction

The asymmetric distribution of charges in the unit cell of ferroelectric (FE) materials induces a directional spontaneous polarization that can be switched by applying an external electric field. This process is essential for different type of applications such as sensors[1,2], actuators[2], memories [3], spintronic devices [4,5], capacitors [6,7] or solar cells [8,9], where FE materials are mostly used in the form of thin films. In the case of solar cells, photon absorbers made of ferroelectrics can be particularly interesting because of the intrinsic internal field brought by the polarization of the material. Such internal fields are very efficient for exciton splitting as needed in photovoltaic devices. Specifically, the polarization of FE materials can induce a large open-circuit voltage that can be several orders of magnitude larger than the bandgap of the absorber leading to large conversion efficiencies. One of the most well-known FE materials is  $\text{BiFeO}_3$  (BFO) that has attracted a lot of attention due to its large electric and magnetic transition temperatures of  $T_c \sim 1100$  K and  $T_N \sim 640$  K,

respectively. Because of its antiferromagnetic character, the applications in magnetism are to date rather limited. However, several studies suggested the use of BFO materials in photovoltaic cells. The relatively large bandgap of BFO (between 2.4 and 3 eV) has nevertheless limited the current flowing through the cell. As a consequence, despite a large open circuit voltage that could reach 15 V, the efficiency of BFO-based cells remained until recently below 1 %.[8]

*Ab initio* calculations performed by Baettig *et al.* revealed that by replacing half of the Fe atoms by Cr, the band gap could be reduced to 1.5 eV. The resulting BiFeCrO<sub>6</sub> (BFCO) double perovskite exhibit a polarization of about 80  $\mu\text{C}/\text{cm}^2$ , large enough to split the electron-hole pairs, as well as a ferrimagnetic character with a magnetization of about 160  $\text{emu}/\text{cm}^3$  (i.e. 2  $\mu_{\text{B}}$  per formula unit)[10]. It was reported that the films exhibited ferroelectricity due to 6  $s^2$  lone pairs on the Bi<sup>3+</sup> and ferrimagnetism due to the super-exchange coupling between Fe<sup>3+</sup> and Cr<sup>3+</sup> [11,12]. In such conditions, Nechache *et al.* managed to grow high-quality epitaxial BFCO thin films on SrTiO<sub>3</sub>(001) substrates using the pulsed laser deposition (PLD) method[13]. Moreover, by controlling the Fe-Cr order through the laser-modulation frequency during the deposition, a controlled variation of the gap was found possible. Thus, by stacking BFCO layers with different bandgaps a multijunction-like solar cell with a power conversion efficiency to 8.1 % under AM 1.5 G irradiation could be obtained[11]. In the case of single BFCO absorption layer, the cell efficiency was about 3.1 %, larger than the 1.25 % record efficiency obtained previously on a Pb(Zr,Ti)O<sub>3</sub>-based FE cell.[14] Since then, Tiwari *et al* succeed to fabricate a solution processed BFO-based solar cell showing an efficiency of about 4%. The band gap of BFO was reduced to 2.2 eV and the thickness of the absorber layer was about 1.5  $\mu\text{m}$ [15]. Although these results are encouraging many structural and ferroelectric details still need to be understood.

In this work, we report on the structural and ferroelectric properties of BFCO thin films grown by PLD on SrTiO<sub>3</sub> (STO) (111) substrates covered with a La<sub>2/3</sub>Sr<sub>1/3</sub>MnO<sub>3</sub> (LSMO) buffer layer. A particular emphasis is given to the polarization switching mechanism which is particularly important in applications such as ferroelectric-based storage devices where the electric resistance of the material is correlated with the local polarization orientation of the film and where the polarization reversal has to be perfectly controlled. The X-ray diffraction measurements reveal an epitaxial growth without spurious phases. The double perovskite superstructure diffraction peaks indicate an Fe-Cr cationic ordering along the growth axis. Atomic force microscopy images show a coalesced grained structure with an average in-plane grain size of about 200 nm. Local measurements realized by piezo-response force microscopy (PFM) show open polarization hysteresis loops, which display an asymmetric polarization switching with respect to the external bias voltage. After poling the BFCO film in opposite directions, PFM imaging reveals stable domains with clear up and down orientations. In addition, the upward poled areas reveal the same contrast as the as-grown regions, indicating a strong preferential polarization orientation in the “up” direction. Statistical PFM measurements performed on different grains show the existence of an internal bias field of relevance for the polarization switching of BFCO. This is observed by asymmetric hysteresis loops with respect to zero applied voltage and found important for the stability of the ferroelectric domain structure.

## Experimental details

Sixty nm thick Bi<sub>2</sub>FeCrO<sub>6</sub> films were grown by PLD on STO (111) substrates covered by a 20 nm thick LSMO layer. LSMO was used as conductive bottom electrode in all PFM experiments. The choice of the (111) orientation for the STO substrate was motivated by the fact that the film polarization can easily align with the growth axis. This axis is also the one along which the FeO and CrO atomic planes

are stacked leading to the periodicity expected in the pseudo-cubic double-perovskite BFCO structure. Besides its good conductive properties LSMO was chosen because of its small lattice mismatch with the respect to the STO substrate. LSMO was grown at 700 °C, in an O<sub>2</sub> atmosphere corresponding to a working pressure of 10 Pa. The laser energy was kept at 30 mJ (fluence of 1.5 J/cm<sup>2</sup>) and the frequency at 5 Hz. For the BFCO deposition, the temperature was 790 °C, the pressure 1 Pa of O<sub>2</sub>, the laser energy 46 mJ (fluence of 2.3 J/cm<sup>2</sup>) and the laser frequency 5 Hz. Other details on the deposition conditions can be found in previous works[11,16,17].

The crystalline structure was investigated by X-ray diffraction (XRD) using a SmartLab Rigaku diffractometer equipped with a Cu source and a Ge (220 × 2) crystal delivering the monochromatic CuKα<sub>1</sub> radiation (0.154056 nm). The high angle measurements (θ-2θ and φ scans) allowed identifying the crystalline structure, checking the phase purity, the Fe-Cr ordering and epitaxial quality of the films. Piezo-response Force Microscopy (PFM) measurements with a vertical polarization sensitivity were performed using a Bruker Icon microscope equipped with a Nanoscope V controller. The microscope was operated out-of-resonance at 40 kHz. The PFM hysteresis loops were acquired by applying V<sub>AC</sub> of 1 V to the LSMO electrode, while recording the phase and amplitude signals as a function of an additional external DC voltage applied to the tip. Probes presenting spring constants of about 80 N/m and tips covered with doped diamond were used all along this study.

## Results and discussion

SrTiO<sub>3</sub> and La<sub>2/3</sub>Sr<sub>1/3</sub>MnO<sub>3</sub> present cubic (Pm-3m; JCPDS card 00-035-0734) and rhombohedral (R-3c; JCPDS card 00-051-0409) structures, respectively. Nevertheless, the LSMO structure is often approximated to a cubic one with a lattice parameter of 3.89 Å (JCPDS card 04-013-6950)[18]. As a consequence, the close symmetry and the small lattice mismatch with respect to STO (bulk lattice parameter of 3.906 Å) allows a layer by layer growth of LSMO on STO[19,20]. As for BFCO, its rhombohedral structure (R3 symmetry) with lattice parameters of a=b= 5.477 Å, c= 13.390 Å and α= 60.09° (JCPDS card 04-011-8839) can be also well approximated with a pseudo-cubic one with lattice parameters of a=b=c= 3.93 Å[16].

Figure 1(a) shows an X-ray diffraction pattern obtained on a BFCO/LSMO/STO(111) sample. As expected, only peaks corresponding to the (111) plane families of STO, LSMO<sub>pc</sub> and BFCO<sub>pc</sub> are observed, indicating a textured growth of LSMO and BFCO on the STO substrate. For a better visibility, a zoom of the X-ray diffractogram around the 111 peak of the substrate is shown in Fig. 1(b). The epitaxial quality of the films was fully confirmed by the φ-scans shown in Fig. 1(c). Upon rotation by 360° around the growth axis, a clear 120°-periodicity is observed for the out of plane peaks indicating an in-plane structural relation between the STO, LSMO and BFCO lattices.

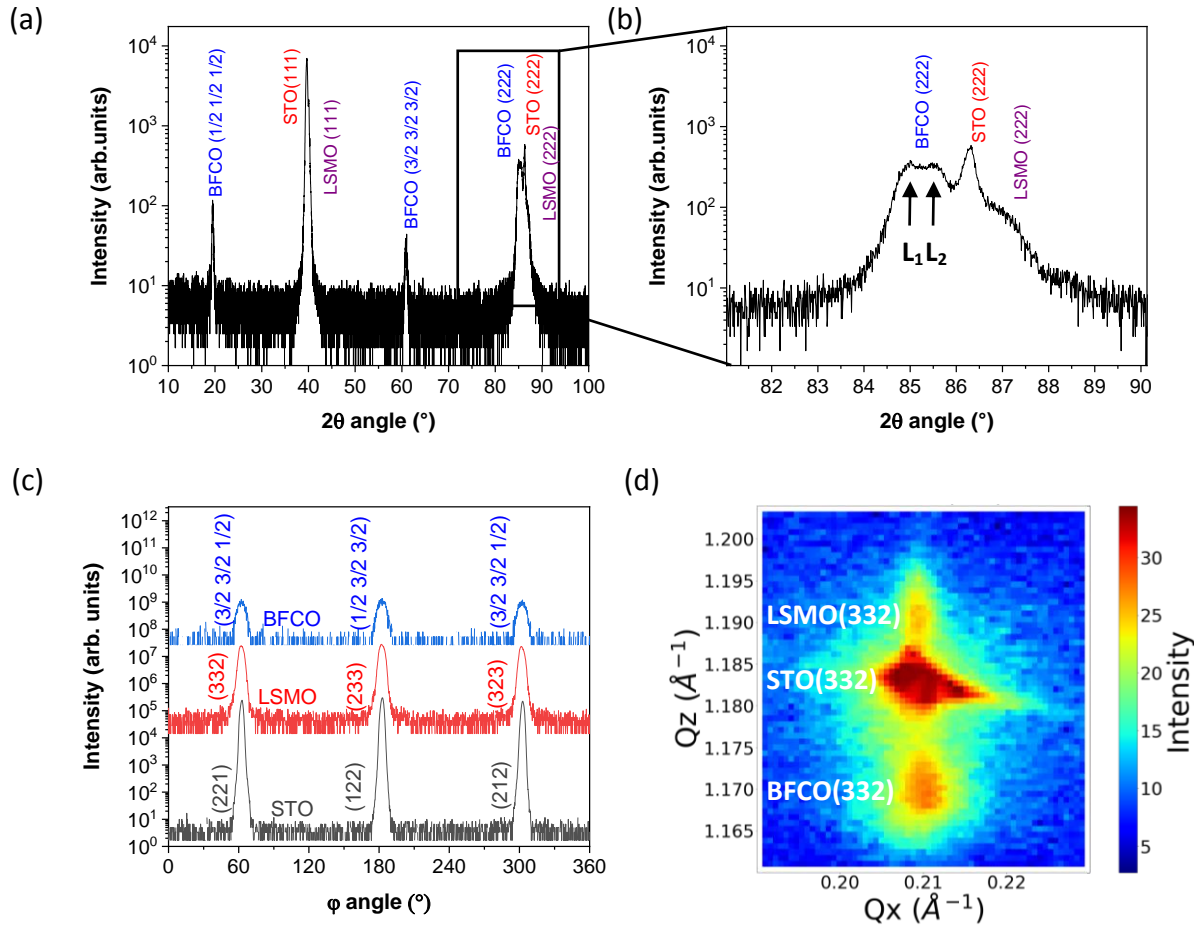


**Fig.1:** (a) X-ray diffraction pattern of a BFCO film (60 nm) deposited on LSMO (20 nm)/STO (111) substrate. The narrow peak at  $20^\circ$  is due to the used monochromator. (b) Zoom on the 111 peak of STO substrate. The BFCO peaks are constituted of two lines, L1 and L2, attributed to Fe-Cr ordered and disordered BFCO phases, respectively. (c)  $\phi$ -scans recorded on the (221)STO peak in grey, (332)LSMO peak in red and (3/2 3/2 1/2) pseudo-cubic BFCO in blue showing a  $120^\circ$  periodicity. (d) Reciprocal space map recorded around the (332) peaks of STO, LSMO and BFCO.

On the basis of the  $\theta$ - $2\theta$  diffractogram presented in Fig.1 (a) the lattice parameters along the growth axis can be calculated for the substrate as well as for both films. As expected, the lattice parameter of the substrate is of  $3.90 \text{ \AA}$  equal to the one reported in the bulk. For LSMO the lattice parameter is slightly smaller ( $3.88(1) \text{ \AA}$ ) than in the bulk and with respect to that of STO [LSMO(222)<sub>pc</sub> peak observed at larger angles[21,22]]. For BFCO instead, the lattice parameter of the thin film is slightly larger than that of STO, as the BFCO(222)<sub>pc</sub> peak is shifted to the left with respect to STO(222) suggesting an in plane compressive strain of BFCO of about 1.2% with respect to the substrate. Interestingly, the BFCO peak seems constituted of two component lines observed at  $85.02^\circ$  (L1) and  $85.48^\circ$  (L2). Such observation was already made on BFCO (100)-oriented films[17,23] and attributed to Fe-Cr cationic ordered (low angle peak) and disordered (high angle peak) phases. This is a first indication that our films are ordered, at least partly. The Fe-Cr cationic order is also evidenced from the presence of the superstructure ( $\frac{1}{2} \frac{1}{2} \frac{1}{2}$ )BFCO and (3/2, 3/2, 3/2)BFCO diffraction peaks observed at  $19.5^\circ$  and about  $60^\circ$ , respectively. This well-defined cationic ordering along the growth direction is

observed despite the similar (3+) valences of Fe and Cr as well by their similar ionic radii[24]. Note finally that no spurious phases could be evidenced within the detection limit of the XRD technique.

In order to analyse the strains of the LSMO and BFCO films on the STO substrate, a reciprocal space map recorded around the 332 peaks of STO, LSMO and BFCO is shown in fig. 1d. As can be observed both the LSMO and BFCO films are perfectly strained on the substrate. This result can be easily understood if we keep in mind the small lattice mismatch between the different layers that do not exceed 1.2% and the small thickness of the layers (20 nm and 60 nm for LSMO and BFCO, respectively).

The surface morphology of the sample was investigated by atomic force microscopy (AFM) at different scales. An example of AFM image is shown in Fig. 2. The film presents a granular structure consisting in coalesced grains with different sizes and shapes. An estimate of the average grain size results in a mean lateral extension of about 200 nm. The height of the grains ranges between approximately 20 and 80 nm. Such a granular morphology can be the result of the interfacial mismatch and the strain effects, in agreement with other film morphologies reported in literature [25,26].

The relatively large lateral sizes of the grains allowed acquiring PFM hysteresis loops at specific locations with respect to the grains. In particular, in this study we chose to locate the tip apex in contact with the centre of well identified grains. This procedure strongly reduces the grain boundary effects and the variability between the hysteresis loops, since the size of the tip apex is smaller than the grain lateral size.

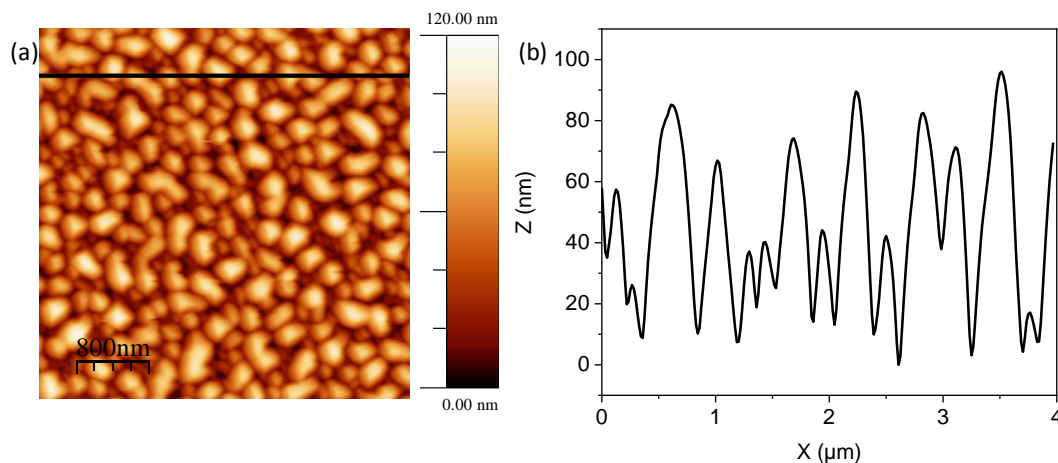


**Fig. 2:** (a) AFM topographic image ( $4 \times 4 \mu\text{m}^2$ ) of BFCO grown atop the LSMO/STO (111) substrate. (b) Scan profile along the solid line from (a), revealing the lateral extension and height of the grains.

Examples of phase-voltage PFM hysteresis loops acquired on different grains are shown in Fig. 3 (a). The corresponding amplitude loops are presented in Fig. 3 (b). Both phase and amplitude signals show open hysteresis and asymmetric shapes with respect to zero voltage. This asymmetry can be quantified by the shift of the centre of the loops which in a large majority is towards positive voltage values. The voltage values corresponding to the left and right switching fields are identical in phase and amplitude signals. The exact values can be found from the curves recorded while changing the bias voltage from low to high values (black) and from high to low values (red). The fact that the switching fields are at the same voltage values in phase and amplitude hysteresis loops is expected for a FE material. However, as shown in Fig. 3, there are variabilities between the grains, as the shift on the voltage axis (labelled as  $V_{\text{bias}}$ ) and opening of the loops depend on the grain.

As a consequence, although a majority of grains exhibits an asymmetric hysteresis loop, the centre of the loops, i.e.  $V_{\text{bias}}$  value, varies from grain to grain asking for a statistical analysis. Such a statistical study resulting from 32 different grains is shown in Fig. 4. An average shift of the loops of  $\langle V_{\text{bias}} \rangle = +1.0$  V and a large variability is observed. Such a shift of the hysteresis loops, is reminiscent of an imprint effect [27,28], which may have different origins, such as strong strain effects generating uniaxial gradient field variation across the film thickness, surface electrostatic effects induced by surface charges, or interfacial built-in electric fields. However, in this system strong strain gradients are not expected since the lattice mismatch between the BFCO and the LSMO/STO substrate is small and the BFCO film is fully strained on the substrate. Biasing effects due to surface charges can also be excluded since there are no changes after multiple scans of the surface with a grounded tip. The interfacial built-in voltage is therefore of particular interest in the present system, as discussed later. The average voltage value corresponding to the centre of the loops  $\langle V_{\text{bias}} \rangle$  can be considered as a measurement of the impact of the built-in potential on the polarization switching. However, the variations of the measured  $V_{\text{bias}}$  cannot be lined to variations of the interface properties which are expected to mainly depend on the nature and structure of the two materials in contact. In fact, the barrier at the BFCO/LSMO interface must be more or less constant, generating a rather constant electric field, regardless of the lateral position. Nevertheless, the impact of such a constant electric field on the polarization switching of an individual grain must depend on the grain characteristics and its environment. This impact, quantified by the  $V_{\text{bias}}$ , represents the only experimentally accessible measure of the effect of the interface field. Considering, the large distribution in the size, shape and likely internal defects of the grains, it is therefore not surprising to have a large variation of the measured  $V_{\text{bias}}$  among the grains.

From Fig. 4, it can be deduced that  $V_{\text{bias}}$  ranges from - 4.2 V to + 0.7 V, with the mean value  $\langle V_{\text{bias}} \rangle = 1.0$  V. Indeed, such variations can be assigned to the heterogeneities present in the film and the exact location probed by the tip with respect to the grain boundaries. This may also include other local factors, such as the polarization state of the nearby grains, the surface state of the grain, the local interfacial state with the buffer layer, and the size and morphology of the grain [29]. The built-in interfacial field manifests therefore as an intrinsic preferential polarization direction of the BFCO film, locally acting as a bias field applied to the film, contributing to an upward preferential polarization direction of the film.

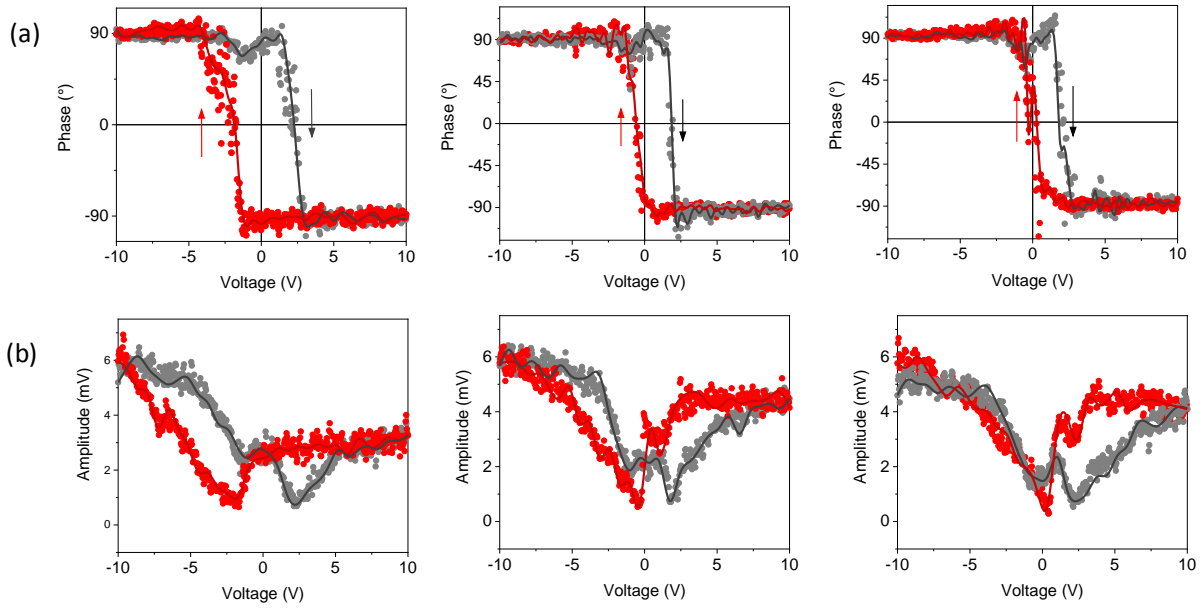


**Fig. 3:** (a) PFM phase vs voltage hysteresis loops acquired above three different grains. Red and black arrows show the sweeping direction of the voltage. (b) Corresponding PFM amplitude vs voltage hysteresis loops.

To further describe the polarization reversal behaviour, one can consider that a measured grain is embedded in an upward polarized medium constituted by the neighbouring grains. During the application of the external continuous (DC) voltage, the surrounding medium, which is not in contact with the tip apex, experiences far less electric field because of the field localization at the tip apex. Consequently, regardless of the external voltage, the polarization of the surrounding medium can be considered as polarized in the upward direction, which is a consequence of the intrinsic upward polarization direction.

In order to confirm the stability of the polarization state, we show in Fig. 5 a PFM phase image ( $8 \times 8 \mu\text{m}^2$ ) after locally poling the film. The area was poled down in the centre ( $6 \times 6 \mu\text{m}^2$ ) by a DC voltage of + 8 V applied to the tip, and then poled up in the middle by applying - 8 V to the tip (bright square of  $3 \times 3 \mu\text{m}^2$ ). The phase signal distribution across the whole image is shown in Fig. 5 (b). The possibility to fully reverse the polarization is therefore demonstrated in the central area. The PFM image [Fig. 5 (b)] shows a stable downward polarization direction (dark contrast in the image) with an average PFM phase around  $40^\circ$  [D peak in Fig. 5 (b)]. The bright signal in the centre corresponds to the area which was poled up. It shows a phase signal of about  $220^\circ$  [U +AG peak in Fig. 5 (b)]. Thus, as expected, the phase difference between the down and up poled areas is  $180^\circ$ . The as-grown (AG) polarization state resulting from the periphery of the image in Fig. 5 (a), is also expected to be comprised in the signal given by D + AG peak as the polarization is up. The small peak that can be observed at about  $150^\circ$  corresponds to the phase signal given by the grain boundaries.

The results presented above can therefore be understood by considering an interfacial built-in field arising at the BFCO/LSMO interface. The formation of a Schottky barrier is expected at this interface, as it occurs between the BFCO and the SRO or ITO for example[11]. The LSMO film is thin enough to allow a space charge region across its thickness. In fact, previous studies conducted on other epitaxial FE systems have demonstrated that the polarization switching in ferroelectric films can be controlled by interface built-in fields[30–33]. The reversed process where the polarization influences

the band bending at the interface was also observed[34]. In the case of the BFCO/LSMO sample studied here, this upward preferential polarisation direction agrees with the PFM image of the as-grown region (Fig 5), showing a majority of white grains as compared with the dark grains. The presence of some dark grains, downward polarised, can also be understood as only about 10 % of the analysed loops in the statistical study reveal a downward polarised state.

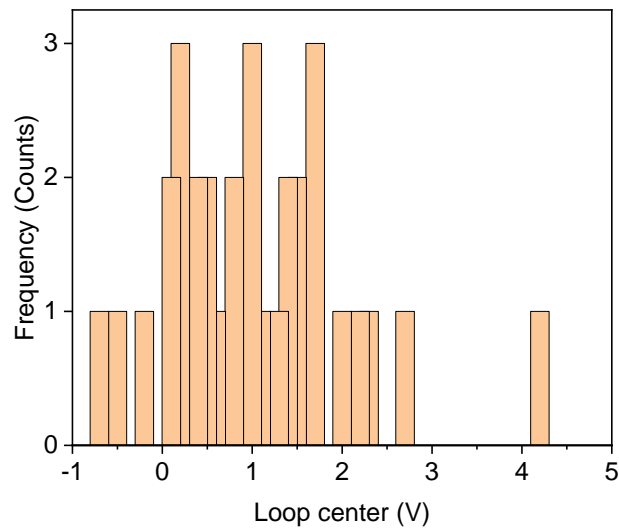


**Fig.4:** Statistical analysis of the centre of the phase loops (i.e.  $-V_{bias}$ ) value obtained by analysing 32 different grains with the same tip and under equivalent measurement conditions. All grains were measured with the same tip and in the same conditions and that loops exhibiting a reproducibility over 3 consecutive acquisitions were used.

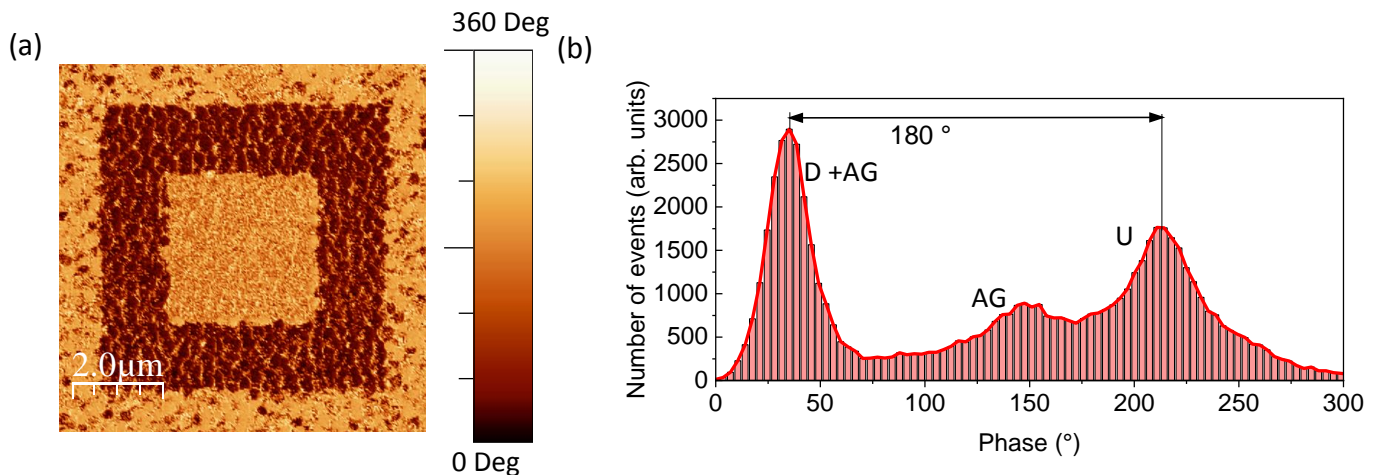


**Fig.5:** (a) PFM phase image ( $8 \times 8 \mu\text{m}^2$ ) of the BFCO film grown on LSMO/STO after poling down an area of  $6 \times 6 \mu\text{m}^2$  at  $V_t = +8 \text{ V}$  (larger square), and then a smaller one of  $3 \times 3 \mu\text{m}^2$  in the up-direction  $V_t = -8 \text{ V}$  (inner square). (b) Phase diagram of the area imaged in (a), revealing the distribution of phase signal, and the  $180^\circ$  phase difference between the up and down polarized zones. The small peak at about  $150^\circ$  corresponds to an intermediate phase signal resulting from grain boundaries.

## Conclusion

Ferroelectric BFCO films were grown by PLD on thin conductive LSMO films deposited on STO(111) substrates. The X-ray diffraction measurements have shown that the BFCO layer is epitaxial, free of spurious phases and showing a correct Fe-Cr cation ordering. AFM and PFM investigations reveal a granular morphology and a preferential upward polarization direction, as well as an asymmetric local hysteresis loop of the polarization, in agreement with the presence of a built-in interfacial field. The impact of the built-in field on the film was estimated by analysing 32 different grains and found to be about  $V_{\text{bias}} = 1$  V. The exact reason why this value varies from grain to grain still remains to be investigated. Nevertheless, the as-grown state is found to be composed of a majority of up-polarized grains which is consistent with the preferential upward polarization direction. Only about 10 % from the grains are found intrinsically down-polarized. The results also indicate a mutual influence between the polarization and the interface bias field.

## Acknowledgment

This work was supported by the French National Research Agency (ANR) through the Programme d'Investissement d'Avenir under contract ANR-11-LABX-0058 - NIE and ANR-17-EURE-0024 within the Investissement d'Avenir program ANR-10-IDEX-0002-02

## References

- [1] D. Damjanovic, P. Muralt, N. Setter, Ferroelectric sensors, *IEEE Sens. J.* 1 (2001) 191–206. <https://doi.org/10.1109/JSEN.2001.954832>.
- [2] P. Muralt, Ferroelectric thin films for micro-sensors and actuators: a review, *J. Micromechanics Microengineering.* 10 (2000) 136–146. <https://doi.org/10.1088/0960-1317/10/2/307>.
- [3] Y. Cho, S. Hashimoto, N. Odagawa, K. Tanaka, Y. Hiranaga, Realization of 10Tbit/in.2 memory density and subnanosecond domain switching time in ferroelectric data storage, *Appl. Phys. Lett.* 87 (2005) 232907. <https://doi.org/10.1063/1.2140894>.
- [4] H. Bea, M. Bibes, G. Herranz, Xiao-Hong Zhu, S. Fusil, K. Bouzehouane, E. Jacquet, C. Deranlot, A. Barthelemy, Integration of Multiferroic BiFeO<sub>3</sub> Thin Films into Heterostructures for Spintronics, *IEEE Trans. Magn.* 44 (2008) 1941–1945. <https://doi.org/10.1109/TMAG.2008.924540>.
- [5] R. Ramesh, A new spin on spintronics, *Nat. Mater.* 9 (2010) 380–381. <https://doi.org/10.1038/nmat2762>.
- [6] W. Ma, Y. Zhu, M.A. Marwat, P. Fan, B. Xie, D. Salamon, Z.-G. Ye, H. Zhang, Enhanced energy-storage performance with excellent stability under low electric fields in BNT–ST relaxor ferroelectric ceramics, *J. Mater. Chem. C.* 7 (2019) 281–288. <https://doi.org/10.1039/C8TC04447C>.
- [7] V. Veerapandiyar, F. Benes, T. Gindl, M. Deluca, Strategies to Improve the Energy Storage Properties of Perovskite Lead-Free Relaxor Ferroelectrics: A Review, *Materials.* 13 (2020) 5742. <https://doi.org/10.3390/ma13245742>.
- [8] S.Y. Yang, J. Seidel, S.J. Byrnes, P. Shafer, C.-H. Yang, M.D. Russell, P. Yu, Y.-H. Chu, J.F. Scott, J.W. Ager, L.W. Martin, R. Ramesh, Above-bandgap voltages from ferroelectric photovoltaic devices, *Nat. Nanotechnol.* 5 (2010) 143–147. <https://doi.org/10.1038/nnano.2009.451>.

- [9] I. Grinberg, D.V. West, M. Torres, G. Gou, D.M. Stein, L. Wu, G. Chen, E.M. Gallo, A.R. Akbashev, P.K. Davies, J.E. Spanier, A.M. Rappe, Perovskite oxides for visible-light-absorbing ferroelectric and photovoltaic materials, *Nature*. 503 (2013) 509–512. <https://doi.org/10.1038/nature12622>.
- [10] P. Baettig, N.A. Spaldin, *Ab initio* prediction of a multiferroic with large polarization and magnetization, *Appl. Phys. Lett.* 86 (2005) 012505. <https://doi.org/10.1063/1.1843290>.
- [11] R. Nechache, C. Harnagea, S. Li, L. Cardenas, W. Huang, J. Chakrabartty, F. Rosei, Bandgap tuning of multiferroic oxide solar cells, *Nat. Photonics*. 9 (2015) 61–67. <https://doi.org/10.1038/nphoton.2014.255>.
- [12] R. Nechache, C. Harnagea, A. Ruediger, F. Rosei, A. Pignolet, EFFECT OF EPITAXIAL STRAIN ON THE STRUCTURAL AND FERROELECTRIC PROPERTIES OF  $\text{Bi}_2\text{FeCrO}_6$  THIN FILMS, *Funct. Mater. Lett.* 03 (2010) 83–88. <https://doi.org/10.1142/S1793604710000981>.
- [13] R. Nechache, C. Harnagea, A. Pignolet, F. Normandin, T. Veres, L.-P. Carignan, D. Ménard, Growth, structure, and properties of epitaxial thin films of first-principles predicted multiferroic  $\text{Bi}_2\text{FeCrO}_6$ , *Appl. Phys. Lett.* 89 (2006) 102902. <https://doi.org/10.1063/1.2346258>.
- [14] F. Zheng, Y. Xin, W. Huang, J. Zhang, X. Wang, M. Shen, W. Dong, L. Fang, Y. Bai, X. Shen, J. Hao, Above 1% efficiency of a ferroelectric solar cell based on the  $\text{Pb}(\text{Zr},\text{Ti})\text{O}_3$  film, *J Mater Chem A*. 2 (2014) 1363–1368. <https://doi.org/10.1039/C3TA13724D>.
- [15] D. Tiwari, D.J. Fermin, T.K. Chaudhuri, A. Ray, Solution Processed Bismuth Ferrite Thin Films for All-Oxide Solar Photovoltaics, *J. Phys. Chem. C*. 119 (2015) 5872–5877. <https://doi.org/10.1021/jp512821a>.
- [16] A. Quattropani, D. Stoeffler, T. Fix, G. Schmerber, M. Lenertz, G. Versini, J.L. Rehspringer, A. Slaoui, A. Dinia, S. Colis, Band-Gap Tuning in Ferroelectric  $\text{Bi}_2\text{FeCrO}_6$  Double Perovskite Thin Films, *J. Phys. Chem. C*. 122 (2018) 1070–1077. <https://doi.org/10.1021/acs.jpcc.7b10622>.
- [17] M.V. Rastei, F. Gellé, G. Schmerber, A. Quattropani, T. Fix, A. Dinia, A. Slaoui, S. Colis, Thickness Dependence and Strain Effects in Ferroelectric  $\text{Bi}_2\text{FeCrO}_6$  Thin Films, *ACS Appl. Energy Mater.* 2 (2019) 8550–8559. <https://doi.org/10.1021/acsaem.9b01465>.
- [18] R. Lyonnet, J.-L. Maurice, M.J. Hÿtch, D. Michel, J.-P. Contour, Heterostructures of  $\text{La}_{0.67}\text{Sr}_{0.33}\text{MnO}_3/\text{SrTiO}_3/\text{La}_{0.67}\text{Sr}_{0.33}\text{MnO}_3$  grown by pulsed laser deposition on (001)  $\text{SrTiO}_3$ , *Appl. Surf. Sci.* 162–163 (2000) 245–249. [https://doi.org/10.1016/S0169-4332\(00\)00199-9](https://doi.org/10.1016/S0169-4332(00)00199-9).
- [19] Z. Liao, M. Huijben, Z. Zhong, N. Gauquelin, S. Macke, R.J. Green, S. Van Aert, J. Verbeeck, G. Van Tendeloo, K. Held, G.A. Sawatzky, G. Koster, G. Rijnders, Controlled lateral anisotropy in correlated manganite heterostructures by interface-engineered oxygen octahedral coupling, *Nat. Mater.* 15 (2016) 425–431. <https://doi.org/10.1038/nmat4579>.
- [20] R. Moubah, S. Colis, C. Ulhaq-Bouillet, M. Drillon, A. Dinia, J. Alaria, Growth and Magnetic Properties of  $\text{La}_{2/3}\text{Sr}_{1/3}\text{MnO}_3/\text{Ca}_3\text{Co}_2\text{O}_6$  Bilayers, *J. Phys. Chem. C*. 114 (2010) 1684–1688. <https://doi.org/10.1021/jp909893n>.
- [21] E.-J. Guo, T. Charlton, H. Ambaye, R.D. Desautels, H.N. Lee, M.R. Fitzsimmons, Orientation Control of Interfacial Magnetism at  $\text{La}_{0.67}\text{Sr}_{0.33}\text{MnO}_3/\text{SrTiO}_3$  Interfaces, *ACS Appl. Mater. Interfaces*. 9 (2017) 19307–19312. <https://doi.org/10.1021/acsami.7b03252>.
- [22] P. Zhou, Y. Qi, C. Yang, Z. Mei, A. Ye, K. Liang, Z. Ma, Z. Xia, T. Zhang, Magnetic anisotropy of epitaxial  $\text{La}_{2/3}\text{Sr}_{1/3}\text{MnO}_3$  thin films on  $\text{SrTiO}_3$  with different orientations, *AIP Adv.* 6 (2016) 125044. <https://doi.org/10.1063/1.4972955>.
- [23] R. Nechache, W. Huang, S. Li, F. Rosei, Photovoltaic properties of  $\text{Bi}_2\text{FeCrO}_6$  films epitaxially grown on (100)-oriented silicon substrates, *Nanoscale*. 8 (2016) 3237–3243. <https://doi.org/10.1039/C5NR08819D>.
- [24] R.D. Shannon, Revised effective ionic radii and systematic studies of interatomic distances in halides and chalcogenides, *Acta Crystallogr. Sect. A*. 32 (1976) 751–767. <https://doi.org/10.1107/S0567739476001551>.
- [25] R. Nechache, C.V. Cojocar, C. Harnagea, C. Nauenheim, M. Nicklaus, A. Ruediger, F. Rosei, A. Pignolet, Epitaxial Patterning of  $\text{Bi}_2\text{FeCrO}_6$  Double Perovskite Nanostructures: Multiferroic at

- Room Temperature, *Adv. Mater.* 23 (2011) 1724–1729.  
<https://doi.org/10.1002/adma.201004405>.
- [26] R. Nechache, F. Rosei, Recent progress in nanostructured multiferroic Bi<sub>2</sub>FeCrO<sub>6</sub> thin films, *J. Solid State Chem.* 189 (2012) 13–20. <https://doi.org/10.1016/j.jssc.2012.01.022>.
- [27] G.H. Kim, H.J. Lee, A.Q. Jiang, M.H. Park, C.S. Hwang, An analysis of imprinted hysteresis loops for a ferroelectric Pb(Zr,Ti)O<sub>3</sub> thin film capacitor using the switching transient current measurements, *J. Appl. Phys.* 105 (2009) 044106. <https://doi.org/10.1063/1.3078104>.
- [28] R. Mahendiran, N. Iyandurai, A. Rajesh, Size and shape effects on polarization reversal of nanoscale BaTiO<sub>3</sub>, *Ferroelectrics.* 572 (2021) 60–70.  
<https://doi.org/10.1080/00150193.2020.1868873>.
- [29] J.S. Liu, S.R. Zhang, H.Z. Zeng, C.T. Yang, Y. Yuan, Coercive field dependence of the grain size of ferroelectric films, *Phys. Rev. B.* 72 (2005) 172101.  
<https://doi.org/10.1103/PhysRevB.72.172101>.
- [30] M.D. Glinchuk, E.A. Eliseev, A.N. Morozovska, Influence of Built-In Internal Electric Field on Ferroelectric Film Properties and Phase Diagram, *Ferroelectrics.* 354 (2007) 86–98.  
<https://doi.org/10.1080/00150190701454628>.
- [31] M. Yang, A. Kc, A.C. Garcia-Castro, P. Borisov, E. Bousquet, D. Lederman, A.H. Romero, C. Cen, Room temperature ferroelectricity in fluoroperovskite thin films, *Sci. Rep.* 7 (2017) 7182.  
<https://doi.org/10.1038/s41598-017-07834-0>.
- [32] M. Stengel, D. Vanderbilt, N.A. Spaldin, Enhancement of ferroelectricity at metal–oxide interfaces, *Nat. Mater.* 8 (2009) 392–397. <https://doi.org/10.1038/nmat2429>.
- [33] C. Lichtensteiger, C. Weymann, S. Fernandez-Pena, P. Paruch, J.-M. Triscone, Built-in voltage in thin ferroelectric PbTiO<sub>3</sub> films: the effect of electrostatic boundary conditions, *New J. Phys.* 18 (2016) 043030. <https://doi.org/10.1088/1367-2630/18/4/043030>.
- [34] B.C. Huang, Y.T. Chen, Y.P. Chiu, Y.C. Huang, J.C. Yang, Y.C. Chen, Y.H. Chu, Direct observation of ferroelectric polarization-modulated band bending at oxide interfaces, *Appl. Phys. Lett.* 100 (2012) 122903. <https://doi.org/10.1063/1.3691615>.